The Infrared Spectrum of PF_3 and Analysis of Rotational Energy Clustering Effect

Barry P. Mant[a], Katy L. Chubb[a], Andrey Yachmenev[b,c], Jonathan Tennyson[a] and Sergei N. Yurchenko[a]

[a]Department of Physics and Astronomy, University College London, London, WC1E 6BT, UK
[b]The Hamburg Center for Ultrafast Imaging, Universitt Hamburg, Luruper Chaussee 149, 22761 Hamburg, Germany
[c]Center for Free-Electron Laser Science (CFEL), Deutsches Elektronen-Synchrotron DESY, Notkestrasse 85, 22607 Hamburg, Germany

ARTICLE HISTORY
Compiled January 31, 2019

ABSTRACT
The first variational calculation of the rotational-vibrational levels of PF_3 are performed and intensities for dipole transitions between them computed. This is accomplished using new state of the art potential energy and dipole moment surfaces. This allows the infrared spectrum of PF_3 to be simulated, providing a complete overview of the ro-vibrational spectrum up to $J = 100$ in the wavenumber range 0–3100 cm^{-1}. The behaviour of PF_3 at high rotational excitations is also investigated. The formation of quasi-degenerate 6-fold rotational energy clusters at high rotational excitation are investigated up to $J = 270$ and are found to occur around $J = 200$. The clustering effect is analysed in terms of semi-classical rotational energy surfaces.

KEYWORDS
molecular data; infrared spectra; rotational energy clustering; phosphorus trifluoride

1. Introduction

Phosphorus trifluoride, PF_3, is a colourless, odourless and highly toxic gas [1] which can bind with haemoglobin in blood in a similar way to carbon monoxide as it is able to act as a pi-acceptor ligand in metal complexes [1–3]. As a triagonal-pyramidal, oblate symmetric top with C_{3v} point group symmetry at equilibrium and the molecular symmetry group $C_{3v}(M)$ [4], the molecular structure of PF_3 is similar to ammonia, NH_3 [5, 6], or phosphine, PH_3 [7]. The inversion barrier for PF_3 is high in energy with early calculations suggesting over $hc \times 40,000$ cm^{-1} [8, 9] while a DFT approach suggested around $hc \times 20,000$ cm^{-1} [10]. Interestingly, the lowest energy planar structure has been suggested to have a C_{2v} symmetry [10, 11] rather than D_{3h} as for NH_3. With a large barrier, inversion motion in PF_3, which is well known to occur in ammonia [12] and potentially in phosphine [13], is suppressed.

PF_3 has been the subject of spectroscopic study for decades [14–20] and research on this molecule remains active [21–26]. The four fundamental bands have been well

characterised [20–22, 26–29] as well as a number of overtone [23, 24, 30] and combination [28, 31, 32] bands. The dense spectrum has in some instances made it difficult to comprehensively study some bands [30]. The microwave rotational spectrum has also been rather well studied [17, 27, 33–36]. Very recently a study of vibrational and electronic inelastic electron scattering on PF_3 has been reported [37].

There has also been limited theoretical work carried out on PF_3. Breidung, *et al.* computed a force field at the Hartree-Fock level of theory as part of a study of phosphorus containing compounds [38]. More recently, Ceausu-Velcescu *et al.* computed a quadratic and cubic force field and other spectroscopic constants using a variety of coupled cluster methods, including the explicitly correlated coupled cluster CCSD(T)-F12b method [26].

In this paper we carry out the first variational calculation of the rotational-vibrational levels of PF_3 and compute intensities for dipole transitions between them. This is accomplished using new state of the art potential energy and dipole moment surfaces (PES and DMS respectively). This allows the infrared spectrum of PF_3 to be simulated, providing a complete overview of the ro-vibrational spectrum with the level of rotational excitation up to $J = 100$ and vibrational band centers covering the range 0–3100 cm^{-1}.

We also investigate theoretically the behaviour of PF_3 at high rotational excitations. Rotational energy clustering is a phenomenon whereby several symmetrically equivalent stable axes of rotation form at high rotationally excited energies. These highly excited rotational states are said to form near-degenerate energy clusters. Rotational energy clustering has been observed theoretically for XY_2 molecules [39] such as H_2S [40], H_2Se [41, 42], and H_2Te [43, 44], and more recently for XY_3 molecules; in the ground excited state for PH_3 [45], SO_3 [46], BiH_3 and SbH_3 [47], and in excited vibrational states for BiH_3 and SbH_3 [47]. Experimentally, rotational energy clustering was confirmed for H_2Se by Kozin *et al.* [48] and Flaud *et al.* [49]. It has also been theoretically predicted to occur in spherical tops such as CF_4 [50, 51], CH_4 [52], and SiH_4 [52, 53]. It has been observed experimentally in SF_6 [54]. However transitions between very highly excited rotational states will be very weak and so bring observational challenges. Novel experimental methods, such as optical centrifuge, should now be capable of generating and studying the rotationally-induced chirality [55], an intriguing phenomena characteristic for molecules with rotational energy clustering. In this work we use similar methods to previous studies [45–47], allowing direct comparisons to be made between different molecules and the behaviour that drives the clustering effect.

Our motivation to study high rotational excitations in PF_3 is to find molecules for which the rotational clustering effects could be observable. PF_3 is a heavy molecule with a small rotational constant, which should easily populate states high values of J. The question however is whether the molecular bonds are flexible enough to allow for the centrifugal effects to stabilize the rotational motion of PF_3 at reasonable energies, in the same way as it is found to stabilize the high J rotations of PH_3, BiH_3 or SbH_3. We also note that gas phase experiments, such as the above mentioned spectroscopic studies on PF_3, have already been carried out and so it would seem a suitable molecule to work with. None of the previously mentioned studies into the microwave and terahertz spectrum of PF_3 have, thus far, detected rotational clustering experimentally.

The paper is organised as follows. In Section 2 we describe how the PES and DMS were constructed and give details of the variational nuclear motion and transition intensity calculations. In Section 3 we compare the results of our *ab initio* calculations of vibrational and rotational energies to experimental values, and discuss the partition

function. We then present simulations of the room temperature PF_3 spectrum as both idealised 'stick' spectra and with broadened lines to give cross sections. The investigation into rotational energy clustering is given in Section 4 and semi-classical analysis of the rotational energy surface is carried out in Section 5. We present conclusions in Section 6.

2. Methods

2.1. Potential Energy Surface

A new *ab initio* potential energy surface is used for this work which was calculated using the explicitly correlated coupled cluster method, CCSD(T)-F12b [56]. The F12-optimized correlation consistent polarized valence cc-pVTZ-F12 [57] basis set was used in the frozen core approximation. A Slater geminal exponent of $\beta = 1.0\ a_0^{-1}$ was used [58]. For the resolution-of-the-identity approximation to the many-electron integrals, we utilized the OptRI [59] basis set. The additional many-electron integrals required for explicitly correlated methods were calculated using the density fitting approach, for which we employed cc-pV5Z/JKFIT [60] and aug-cc-pwV5Z/MP2FIT [61] auxiliary basis sets. All calculations were carried out using MOLPRO2012 [62]. Electronic energies were calculated on a grid of about 20 000 molecular geometries for energies of up to $hc \times 40\,000\ \mathrm{cm}^{-1}$ above the equilibrium geometry value.

We employed a Morse-type parametrised potential energy function,

$$V(y_1, y_2, y_3, y_4, y_5, y_6) = \sum_{i,j,k,\ldots} c_{ijkl\ldots} y_i y_j y_k y_l \cdots . \tag{1}$$

This is expressed in terms of three stretching variables

$$y_1 = 1 - \exp\left(-a(r_1 - r_\mathrm{e})\right), \tag{2}$$
$$y_2 = 1 - \exp\left(-a(r_2 - r_\mathrm{e})\right), \tag{3}$$
$$y_3 = 1 - \exp\left(-a(r_3 - r_\mathrm{e})\right), \tag{4}$$

with equilibrium $r_\mathrm{e} = 1.56$ Å and the Morse parameter $a = 1.0\ \mathrm{Å}^{-1}$; two symmetrized bending variables

$$y_4 = \frac{1}{\sqrt{6}}(2\alpha_1 - \alpha_2 - \alpha_3) \tag{5}$$
$$y_5 = \frac{1}{\sqrt{2}}(\alpha_2 - \alpha_3). \tag{6}$$

and the 'umbrella' coordinate

$$y_6 = \frac{2}{\sqrt{3}} \sin[(\alpha_1 + \alpha_2 + \alpha_3)/6]. \tag{7}$$

These are similar to the variables used for the potential function of BiH_3 and SbH_3 [47], PH_3 [63–65], NH_3 [66], OH_3^+, CH_3^+ [67], CH_3 [68] and SO_3[69]. The bond lengths, r_1, r_2, r_3, are the instantaneous distances between the central P atom and each of the F atoms, respectively. α_i denotes the bond angle $\angle(F_j P F_k)$ where (i, j, k) is a

permutation of the numbers (1,2,3) (see Figure 1). The root-mean-square error for the fit of this potential was of the order of 1 cm^{-1}, up to 10,000 cm^{-1}. Although not the focus of this work, we have used our PES to investigate the inversion barrier. At planar geometries our PES gives a barrier of around 32,500 cm^{-1} relative to equilibrium for the D_{3h} geometry reported by Gutsev [10] with a slightly lower energy of 31,000 cm^{-1} for the C_{2v} geometry. The PES is given as a Fortran 90 subroutine in the supplementary information.

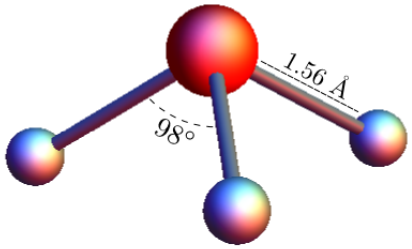

Figure 1. Equilibrium configuration of PF_3.

2.2. Dipole Moment Surface

A new *ab initio* dipole moment surface was used for this work, calculated using MOLPRO at CCSD(T) level of theory with an aug-cc-pVTZ basis set in the finite field approximation. For each of the x, y and z Cartesian components an electric field of strength ± 0.001 a.u. was applied and the dipole moment projections μ_x, μ_y and μ_z computed as derivatives of the electronic energy with respect to the field strength using central finite differences. Calculations were carried out using the same grid as for computing the *ab initio* potential energy surface. The dipole moment function was of a similar form to that of PH_3 utilising the Molecular-Bond (MB) representation [70]. In the MB representation the electronically averaged dipole moment vector, $\bar{\mu}$ is given as

$$\bar{\mu} = \bar{\mu}_1^{\text{Bond}}\mathbf{e}_1 + \bar{\mu}_2^{\text{Bond}}\mathbf{e}_2 + \bar{\mu}_3^{\text{Bond}}\mathbf{e}_3 \tag{8}$$

where the $\bar{\mu}_i^{\text{Bond}}$ are three functions of vibrational coordinates and $\mathbf{e}_i$ is a unit vector along the P-F_i bond,

$$\mathbf{e}_i = \frac{\mathbf{r}_i - \mathbf{r}_4}{|\mathbf{r}_i - \mathbf{r}_4|} \tag{9}$$

with $\mathbf{r}_i$ the position vector of F_i and $\mathbf{r}_4$ the position vector of the phosphorus nucleus.

Due to the symmetry of the molecule all three projections of the dipole can be expressed as a single function $\bar{\mu}^{(0)}(r_1, r_2, r_3, \alpha_1, \alpha_2, \alpha_3)$ such that

$$\begin{aligned}
\bar{\mu}_1^{\text{Bond}} &= \bar{\mu}^{(0)}(r_1, r_2, r_3, \alpha_1, \alpha_2, \alpha_3) \\
\bar{\mu}_2^{\text{Bond}} &= \bar{\mu}^{(0)}(r_2, r_1, r_3, \alpha_2, \alpha_1, \alpha_3) \\
\bar{\mu}_3^{\text{Bond}} &= \bar{\mu}^{(0)}(r_3, r_2, r_1, \alpha_3, \alpha_2, \alpha_1).
\end{aligned} \tag{10}$$

This is expanded as

$$\bar{\mu}^{(0)}(\xi_1,\xi_2,\xi_3,\xi_4,\xi_5,\xi_6) = \mu^{(0)} + \sum_k \mu_k^{(0)}\xi_k + \sum_{k,l} \mu_{kl}^{(0)}\xi_k\xi_l + \sum_{k,l,m} \mu_{klm}^{(0)}\xi_k\xi_l\xi_m + \dots \quad (11)$$

The function $\bar{\mu}^{(0)}$ is expressed in terms of the same three stretching variables, relating to bond lengths r_1, r_2 and r_3, and equilibrium bond length r_e (which is common for all three bonds) as the PES, along with Morse parameter, $\beta = 1.0$ Å^{-1} and the three α_i angles with $\alpha_\mathrm{e} = 98.0°$ such that

$$\xi_i = (r_i - r_\mathrm{e}) \exp\left(-\beta^2 (r_i - r_\mathrm{e})^2\right) \qquad (i = 1, 2, 3) \quad (12)$$

$$\xi_j = \cos\left(\alpha_{j-3}\right) - \cos\left(\alpha_\mathrm{e}\right) \qquad (j = 4, 5, 6) \quad (13)$$

The root-mean-square error for the dipole moment fit was of the order of 10^{-4} Debye. At equilibrium our fitted DMS gives a dipole moment of 0.93 D. This is in reasonable agreement with the values calculated by Ceausu-Velcescu *et al.* of 0.985 D at the CCSD(T)/AWCVQZ level of theory (0.955 D using frozen core approximation) and the experimental value of 1.029(1) D [71].

The DMS is given as a Fortran 90 subroutine in the supplementary information.

2.3. Variational Calculations

Variational ro-vibrational calculations were carried out using the TROVE program. The TROVE methodology is well documented [72–76] and has been applied to a variety of molecules, mostly as part of the ExoMol project [7, 65, 69, 73, 77–85]. Only the specific details relevant to this work on PF_3 will be discussed here.

The ro-vibrational Hamiltonian was constructed numerically as implemented in TROVE [72]. The Hamiltonian was expanded using a power series around the equilibrium geometry of the molecule. The coordinates used were linearised versions of the stretching coordinates; $\xi_i^l = r_i - r_\mathrm{e}$ (i = 1-3) and bending coordinates; $\xi_i^l = \alpha_{i-3} - \alpha_\mathrm{e}$ (i = 4-6). The kinetic energy operator was expanded to 6th order and the potential energy operator to 8th order. Morse coordinates of form $\xi_i^l = 1 - \exp(-a\xi_i^l)$ ($i = 1-3$ and $a = 1.0$ Å^{-1} is the Morse parameter) were used in the potential expansion for the stretching coordinates with the bending coordinates expanded as ξ_i^l (i = 4-6) themselves. Atomic masses were used throughout.

A multistep contraction scheme was used to build the vibrational basis set [75]. For each coordinate ξ_i^l a one-dimensional Schrödinger equation was solved using the Numerov-Cooley approach [72, 86, 87] to generate basis functions $\phi_{n_i}(\xi_i^l)$ with vibrational quantum number n_i. The vibrational basis set functions $|v\rangle$ are formed as products of the 1D basis functions

$$|v\rangle = \prod_\nu |n_\nu\rangle = \phi_{n_1}(\xi_1^l)\phi_{n_2}(\xi_2^l)\phi_{n_3}(\xi_3^l)\phi_{n_4}(\xi_4^l)\phi_{n_5}(\xi_5^l)\phi_{n_6}(\xi_6^l). \quad (14)$$

The basis set is truncated by the polyad number P via

$$P = 2(n_1 + n_2 + n_3) + n_4 + n_5 + n_6 \leq P_\mathrm{max} = 14. \quad (15)$$

A contracted basis set was then formed by reducing the six dimensional problem into two detached subspaces: $(\xi_1^l, \xi_2^l, \xi_3^l)$ for stretching coordinates and $(\xi_4^l, \xi_5^l, \xi_6^l)$ for bending coordinates. A Hamiltonian matrix is constructed and diagonalised for each of these subspaces to give symmetrised contracted vibrational basis functions for the stretching and bending coordinates respectively. The details of this step have been discussed in a recent publication [75]. Products of these eigenfunctions are formed which are also truncated via Eq. (15).

This procedure generated 1455, 1125 and 2571 vibrational eigenfunctions $|\Phi_{\rm vib}^{(i)}\rangle$ for the A_1, A_2 and E states respectively with term energies $\tilde{E}_i^{(J=0)}$ up to 8 000 cm^{-1} above the ground state (with zero point energy of 1901.0 cm^{-1}). As is usual for TROVE, the $J = 0$ contraction scheme is employed for computing states with $J > 0$ [73]. This uses the vibrational eigenfunctions combined with symmetrized rigid-rotor functions as a basis set for $J > 0$ calculations rather than the primitive vibrational functions [73, 75]. As the PF_3 molecule has a relatively large moment of inertia, levels up to high values of J are required to simulate the infrared spectrum, even at modest temperatures. To obtain a manageable basis set size, only vibrational eigenfunctions with term energies less than 3100 cm^{-1} were used in the $J = 0$ contraction. This will make the basis set slightly less flexible compared to using all states but greatly reduce computational time. The most intense bands in the PF_3 spectrum are below 2000 cm^{-1} so limiting the basis to this energy range is reasonable. After this basis truncation 105, 70 and 161 vibrational eigenfunctions for each symmetry are retained. As the vibrational energies were computed with the full $P_{\rm max} = 14$ basis, the accuracy of the vibrational band centres is retained.

As shown in Section 3, the *ab initio* vibrational band centres are mostly in good agreement with the experimental values. The PES could be improved further by refining to the experimental data [6]. This has been carried out for constructing high temperature line lists [7, 80, 81, 83, 84] with the motivation that improving the PES near equilibrium will also improve the PES for higher energies where there is typically less experimental data available. Refinement can be an expensive procedure however, often requiring dozens of PES parameters to be adjusted for multiple values of J [84] and can lead to over fitting if care is not taken [80]. As an alternative, for this room temperature line list where the main adsorption bands occur between 0-2000 cm^{-1}, we replace the calculated vibrational energies with experimental values where possible [88] as the $J = 0$ basis is diagonal with respect to the vibrational component of the Hamiltonian [73]. This should give an accuracy for the vibrational bands in line with the rotational energies (section 3.2).

2.4. Line Intensities

The eigenvectors from the variational calculation along with the DMS were used to compute Einstein-A coefficients of transitions. These satisfy the rotational selection rules [89]

$$J' - J'' = 0, \pm 1, \quad \text{and} \quad J' + J'' \neq 0, \tag{16}$$

where J' and J'' are the upper and lower values of the total angular quantum number J and the C_{3v}(M) symmetry selection rules

$$A_1 \leftrightarrow A_2 \quad \text{and} \quad E \leftrightarrow E. \tag{17}$$

The absolute absorption intensities are then given by [89]

$$I(f \leftarrow i) = \frac{A_{fi}}{8\pi c} g_{\rm ns}(2J_f + 1) \frac{\exp(-c_2 \tilde{E}_i/T)}{Q(T)\tilde{\nu}_{fi}^2} \times \left[1 - \exp\left(-\frac{c_2 \tilde{\nu}_{fi}}{T}\right)\right], \qquad (18)$$

where J_f is the rotational quantum number for the final state, $\tilde{\nu}_{fi}$ is the transition frequency ($\tilde{\nu}_{fi} = \tilde{E}_f - \tilde{E}_i$), $\tilde{E}_i$ and $\tilde{E}_f$ are the initial and upper state term values, respectively, $Q(T)$ is the partition function (Section 3.3), and c_2 is the second radiation constant. The Einstein-A coefficients A_{fi} between the ro-vibrational states i and f have been defined previously [90]. ^{19}F nuclei have a nuclear spin of 1/2 and so the nuclear spin statistical weights $g_{\rm ns}$ for PF_3 are the same as those of phosphine [7]: (8,8,8) for states of symmetry (A_1, A_2, E) respectively, within the HITRAN convention of including the full nuclear spin of each species [91].

The temperature independent Einstein-A coefficients were computed using the GAIN-MPI program [92]. Intensities were computed using a lower energy range of 0 – 4500 cm^{-1} taking into account up to $J = 100$ for transition frequencies between 0 and 4000 cm^{-1}. An intensity cut-off of 10^{-30} cm molecule^{-1} was used at 298 K.

3. Results

3.1. Ab Initio Vibrational Energies

The vibrational energies obtained from the *ab initio* PES with the full $P_{\rm max} = 14$ basis set are shown in Table 1. The results for the ν_2 and ν_4 bands and combinations/overtones of these fundamentals are in good agreement with experimentally derived values. For the ν_1 and ν_3 fundamentals the agreement with experiment is not as good but still reasonable for an *ab initio* PES at the level of electronic structure theory used. To estimate the convergence of vibrational energies with this basis set we used a complete vibrational basis set (CVBS) extrapolation procedure similar to that described by Owens *et al.* [82]. Variational calculations were carried out with $P_{\rm max} = 12, 14$ and 16 basis sets respectively. From this we estimate that the basis set incompleteness error for the $P_{\rm max} = 14$ basis is of the order 10^{-3} cm^{-1} for the fundamental bands and therefore our errors largely come from the approximations made in the *ab initio* calculations of the PES. For the energy range 0-2000 cm^{-1} (the main region of the infrared spectrum) and 0-3100 cm^{-1} (the range of basis functions used for $J > 0$ calculations) the convergence errors are estimated to be around 0.1 and 3.5 cm^{-1} respectively. As discussed above, to obtain a more accurate simulation of the infrared spectrum we replaced the *ab initio* calculated band centres with empirical values [88].

Table 1. Comparison of computed vibrational band origins for PF_3 with the empirical values. Energy term values are in cm^{-1}.

Band	Symmetry	*Ab initio*	Experiment ([25, 88])
ν_1	A_1	895.742	891.940
ν_2	A_1	487.377	487.716
ν_3	E	861.771	859.219
ν_4	E	346.748	347.086
$\nu_2+\nu_4$	E	833.664	834.381
$2\nu_4^0$	A_1	692.286	692.847
$2\nu_4^{\pm 2}$	E	694.039	694.695
$2\nu_2$	A_1	974.830	975.190
$3\nu_4^{\pm 1}$	E	1038.347	1039.071
$3\nu_4^{\pm 3}$	A_1	1041.821	1042.650
$\nu_2+2\nu_4^0$	A_1	1178.665	1179.069
$\nu_2+2\nu_4^{\pm 2}$	E	1180.420	1180.919
$(\nu_3+\nu_4)_{\parallel}$	A_2	1206.483	1204.790
$(\nu_3+\nu_4)_{\perp}$	E	1206.718	1205.068
$2\nu_2+\nu_4$	E	1320.610	1320.788
$\nu_2+\nu_3$	E	1347.158	1345.440
$\nu_1+\nu_2$	A_1	1381.459	1377.754
$\nu_1+\nu_4^{\pm 1}$	E	1240.776	1237.386

3.2. Rotational Energies

To assess the accuracy of our pruned basis set using the $J = 0$ method we compare rotational energies with experimental values for both the ground vibrational state and the $\nu_2 = 1$ state [20, 35]. For $J < 5$ our observed−calculated errors are of the order of $1{\times}10^{-3}$ cm^{-1}. For higher Js (40-60) this increased to $1{\times}10^{-2}$. We thus expect our $J = 100$ rotational energies to still be relatively accurate despite making the $J = 0$ contraction. Our root-mean-square error for all rotational energies compared with experiment are $8.7{\times}10^{-2}$ cm^{-1} for the ground vibrational state and $2.5{\times}10^{-2}$ cm^{-1} for the $\nu_2 = 1$ state.

3.3. Partition Function

The temperature-dependent partition function $Q(T)$ is defined as

$$Q(T) = \sum_i g_i \exp\left(-c_2 \frac{\tilde{E}_i}{T}\right), \tag{19}$$

where $g_i = g_{\rm ns}(2J_i + 1)$ is the degeneracy of the state i with energy E_i and rotational quantum number J_i and c_2 is the second radiation constant.

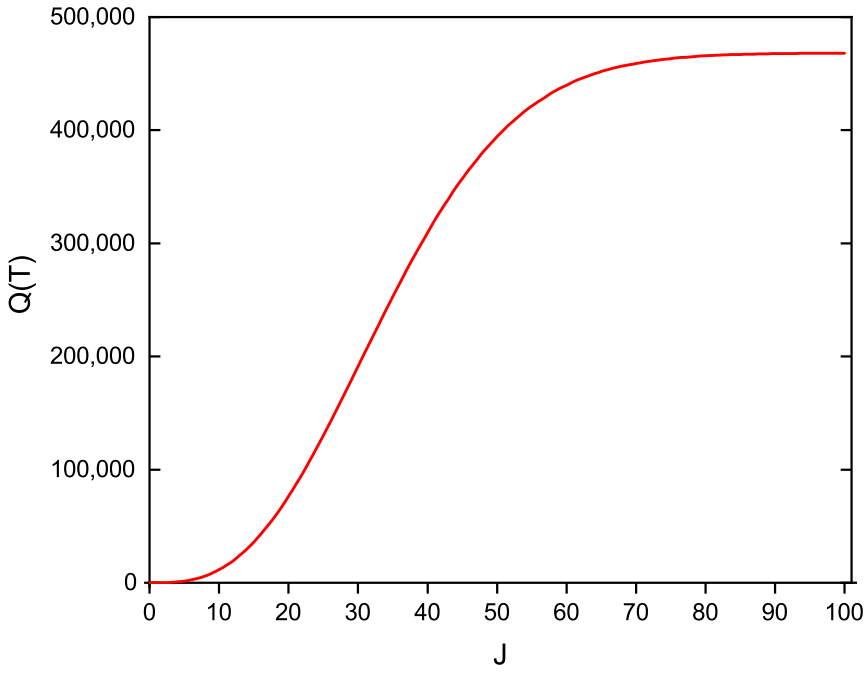

Figure 2. Convergence of partition function of PF_3 at 296 K with respect to the rotational quantum number J.

To the best of our knowledge the PF_3 partition function has not yet been computed. We provide the value of the partition function calculated using our model between 1-400 K on a 1 K grid in the supplementary information. At 296 K the partition function has the value 4.68 $\times 10^5$. Fig. 2 shows the convergence of $Q(T)$ as a function of J at 296 K for up to $J = 100$. The partition function is converged to around 0.1 %. The large mass of the fluorine atoms gives PF_3 a large moment of inertia and so rotational levels are closely spaced in energy. To simulate the infrared spectrum at higher temperatures as is typically done in the ExoMol project would require many Js to be calculated, well past $J = 100$. This was carried out for the SO_3 molecule where up to $J = 130$ was required for 800 K. For PF_3, even higher values of J would be required but this can be carried out using special methods. These include saving the Hamiltonian matrix to disc and diagonalizing using external parallel programs or making use of diagonalizers specially developed for large matrices [46, 85].

3.4. Spectrum Simulations

The PF_3 spectrum can be simulated using the model described above. This results in 68 billion transitions between 3.3 million (3 311 926) states for up to $J = 100$.

An overview of the PF_3 infrared absorption cross section at 296 K is shown in Figure 3 at a resolution of 0.1 cm^{-1} convoluted with a Voigt profile with a half-width half-maximum (HWHM) value of 0.1 cm^{-1} using the Exocross program [93]. There are only transition intensities above 1×10^{-25} cm/molecule for the 0–2000 cm^{-1} frequency range at this temperature. The PF_3 spectrum is dominated by the most intense bands

between 800–930 cm^{-1} corresponding to the ν_1 and ν_3 bands respectively. The weaker ν_2 and ν_4 fundamental bands as well as other overtone and combination bands can also be seen at this scale. As noted by Rey *et al.* in their calculation of the CF_4 spectrum [94], fluorine containing molecules have relatively low vibrational frequencies. This leads to hot bands in the spectrum, even at room temperature, from transitions between excited vibrational states. This is also the case for PF_3 resulting in very congested absorption bands. These hot bands are not visible or indicated in Figure 3 as they are hidden by the more intense bands but are discussed and partially shown below.

Stick spectra are shown in Figure 4. As the PF_3 spectrum is very dense only the strongest transitions on a 0.05 cm^{-1} grid were plotted. To date, only relative absorption intensities for PF_3 have been given in the literature [26–28, 30–32]. The spectra simulations here are the first to give absolute absorption intensities for this molecule.

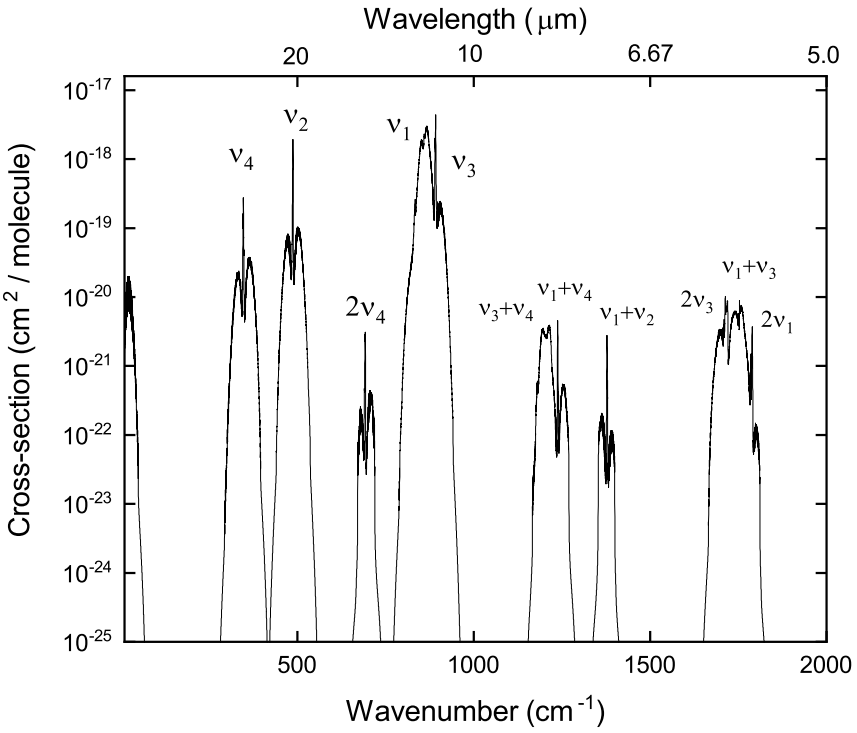

Figure 3. Overview of simulated PF_3 spectrum at 296 K.

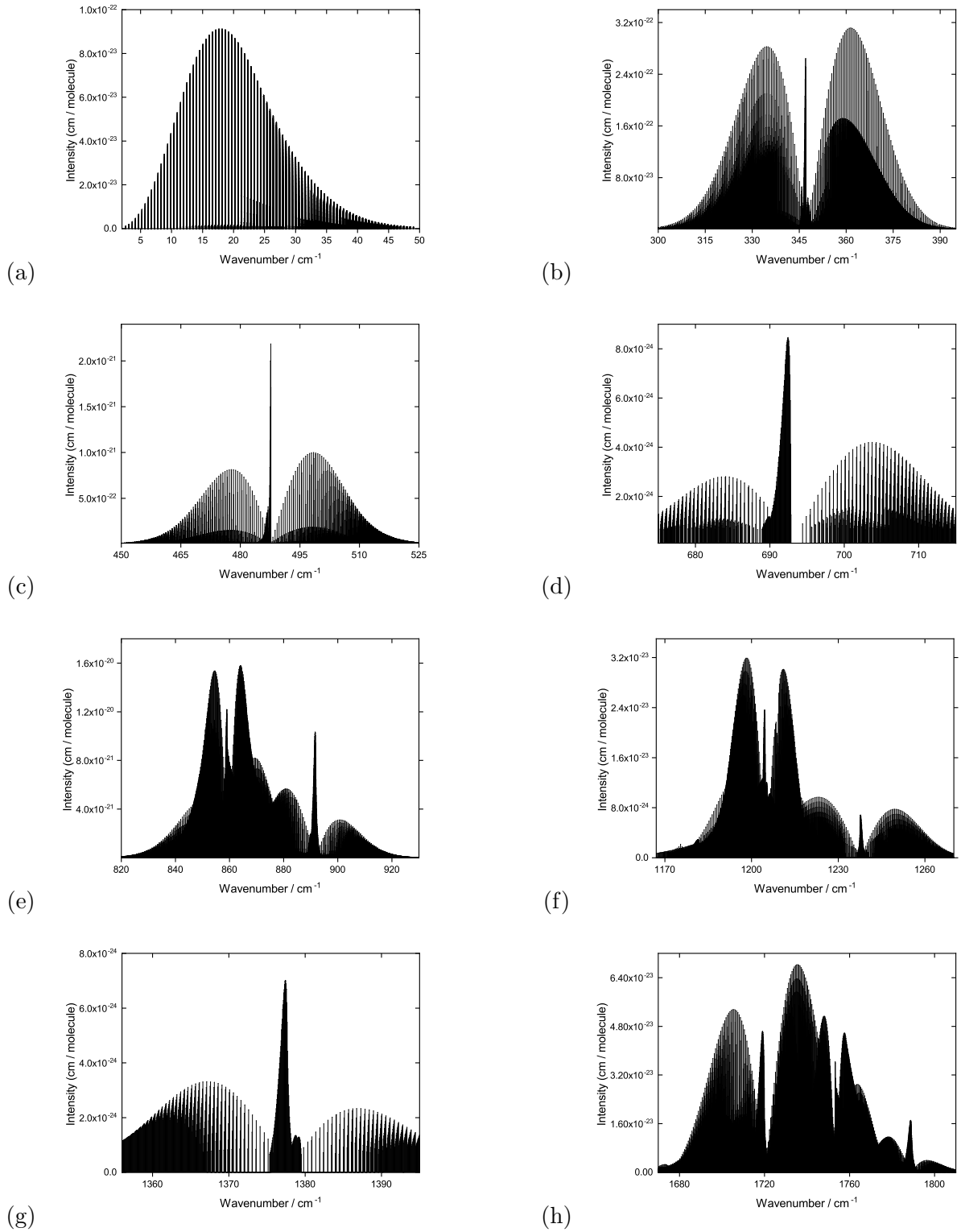

Figure 4. Stick spectra for the main PF_3 absorption bands at 296 K. (a) is pure rotational band, (b),(c) and (e) are fundamental bands and (d),(f),(g) and (h) are overtone and combination bands. Details of each band are given in main text.

The PF_3 molecule has a permanent dipole moment giving an appreciable pure rotational spectrum. This is shown in Figure 4(a). The rotational spectrum peaks at around 18 cm^{-1} at 296 K.

Figure 4(b) shows the spectrum between 300-390 cm^{-1} which is dominated by the ν_4 fundamental band. This has the PQR structure expected for a parallel band.

Figure 4(c) shows the spectrum between 460-510 cm^{-1} which is dominated by the ν_2 fundamental band. The appearance is similar to the $\nu_4 = 1$ band but contains a very sharp and intense Q-branch. This region also contains weaker contributions from the $2\nu_2 - \nu_2$ [28, 88] and $\nu_2 + \nu_4 - \nu_4$ [28, 95] hot bands.

The relatively weak $2\nu_4$ overtone band is shown in Figure 4 (d) between 670-720 cm^{-1}.

Figure 4(e) shows the spectrum between 820–920 cm^{-1}. This region is very dense and contains many transitions. As remarked the ν_1 and ν_3 bands in the region are the most intense of the whole spectrum. The ν_1 band is a parallel band while the ν_3 band is of perpendicular type. As shown below, the $\nu_2 + \nu_4$ band also appears in this region but is not apparent in the 'stick' plot. The ν_1 band has a relatively wide Q branch with hot band Q branches from $(\nu_1 + n\nu_4 - n\nu_4)$ transitions [28]. The R branch of ν_1 significantly overlaps with the ν_3 band.

The spectral range between 1170–1260 cm^{-1} is another dense region as shown in Figure 4(f). The strongest features are the two $\nu_3 + \nu_4$ combination bands and the $\nu_1 + \nu_4$ band. Also contained in this region (but not readily visible on a 'stick' plot) are the $\nu_2 + 2\nu_4^0$, $\nu_1 + 2\nu_4^{\pm 2} - \nu_4^{\pm 1}$ and $\nu_1 + 3\nu_4^{\pm 3} - 2\nu_4^{\pm 2}$ bands [31].

Figure 4 (g) shows the spectrum between 1350–1400 cm^{-1}. The main feature is the $\nu_1 + \nu_2$ combination band. Also in this region (but not observable on the 'stick' plot) are the $\nu_1 + \nu_2 + \nu_4 - \nu_4$ and $\nu_1 + \nu_2 + 2\nu_4 - 2\nu_4$ hot bands [32].

The highest frequency absorption features in the range considered is shown in Figure 4(h) between 1670–1815 cm^{-1}. This is another congested region and to the best of our knowledge has not yet been analysed experimentally. The dominating features of this region are the $2\nu_3$ overtone band at 1719 cm^{-1}, the $\nu_1 + \nu_3$ combination band at 1753 cm^{-1} and the $2\nu_1$ combination band at 1789 cm^{-1}. Due to lack of experimental data, the centres of these bands were not empirically corrected and stayed at the values predicted purely *ab initio*. From Table 1, we expect our predictions to overestimate the positions of the overtone stretching bands centres by about 3–5 cm^{-1}.

The 'stick' spectra plotted in Figure 4 are idealised and do not consider the effects of Doppler and collisional broadening. To simulate the observable spectrum we use a resolution of 0.1 cm^{-1} and broaden the lines with a Voigt profile with a half-width half-maximum (HWHM) value of 0.1 cm^{-1} using the Exocross program [93]. Figure 5 shows the results of this process for the main vibrational bands. From experience [83–85] these parameters are usually sufficient for accurately simulating infrared spectra from the PNNL database [96] (although PF_3 is not yet included in this database). Due to the density of relatively intense lines, these parameters result in very broad features, removing most of the structure from the spectrum.

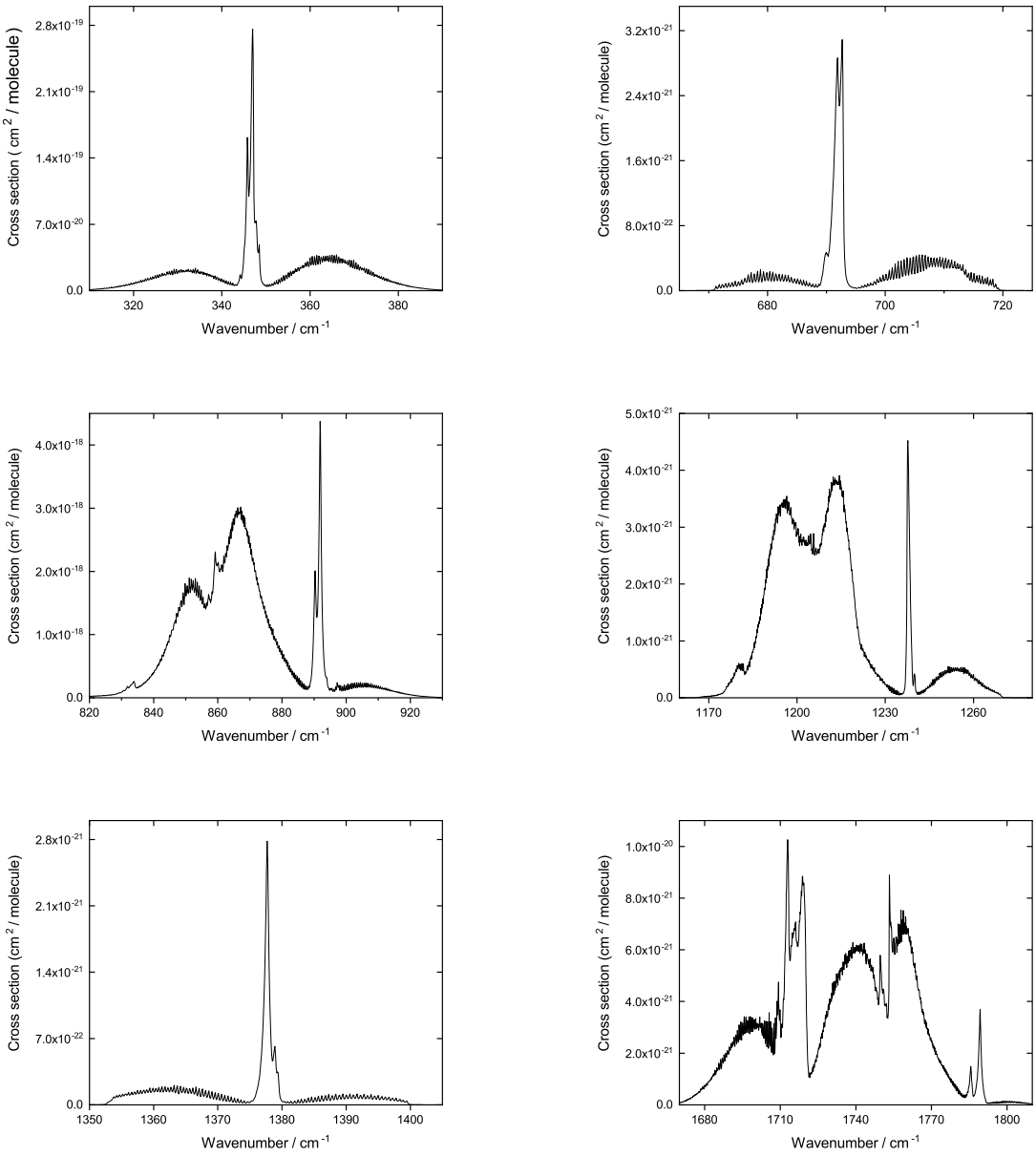

Figure 5. PF_3 spectra convoluted using Voigt profile with hwhm of 0.1 cm^{-1} at 296 K

To the best of our knowledge an experimental spectrum for PF_3 is not currently available as data files in the literature. To provide some comparison to experiment we compare our results the high resolution spectra of Ben Sari-Zizi *et al.* [28, 31]. Figure 6 shows the simulated spectra for the ν_3 and ν_1 fundamental bands (left) and $\nu_3 + \nu_4$ and $\nu_1 + \nu_4$ combination bands (right). For these plots a resolution of 0.01 cm^{-1} was used and lines broadened using a Voigt profile with HMWM of 0.01 cm^{-1}. The left and right plots are in reasonable qualitative agreement with both Figure 1s of references [28] and [31] respectively.

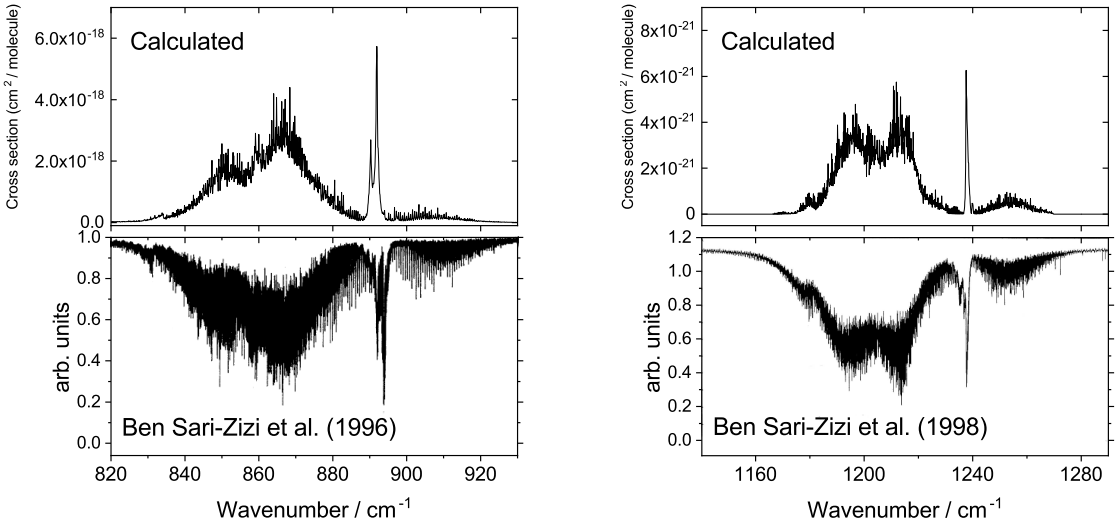

Figure 6. PF_3 spectra convoluted using Voigt profile with HWHM of 0.01 cm^{-1} at 296 K for comparison with Figure 1s of references [28] and [31].

4. Rotational Energy Clustering

Previous theoretical work investigating the behaviour of general XY_2 [39–44], XY_3 [45–47] and XY_4 [50–53] molecules at high rotational excitations have found the emergence of several symmetrically equivalent axes of rotation as the energy is increased. These stable axes of rotation correspond to anticlockwise/clockwise motion about each of the X-Y bonds.

We have computed rotational term values (energies) for the ground vibrational state of PF_3, using variational calculations similar to those outlined in Section 2.3 but for a much lower basis set ($P_{\max} = 6$ for Eq. (15)), for $J \leq 270$ (corresponding to 17,500 cm^{-1}). The lower basis set was sufficient to converge the purely rotational states of PF_3 to 10^{-2} cm^{-1} or better for $J = 0..100$. Although the convergence error gradually builds up with increasing J up to 270 we believe that this is effectively negligible for the purpose of the rotational clustering analysis. Due to the stabilisation of the rotational motion, characterised by rotational clustering, the interaction of rotation with the vibration becomes less important, justifying the smaller vibrational basis set. This is a qualitative effect in the vibrational ground states, which is not very sensitive to the size of the vibrational basis set [45]. Equilibrium values of $r_e = 1.56$ Å and α_e=98° were used for the bond lengths and bond angles, respectively. The rotational term values, in the $\nu = 0$ vibrational ground state, are given by $\tilde{E}_{J,K}$ with K representing the projection of the angular momentum, J, onto the molecular z-axis (see Figure 1). In order to illustrate the cluster formation, the rotational term value spacings, $\tilde{E}_{J,K} - \tilde{E}^{\max}_{J,K}$, are plotted against J in Figure 7, where $\tilde{E}^{\max}_{J,K}$ is the maximum energy (this occurs at $K = K_a$=0 and $K = K_c$=0) for a given value of J, as a function of K, in the ν=0 vibrational ground state. As can be seen in Figure 7, each cluster is formed from four distinct states, colour-coded by their symmetry, which span the reducible

representation

$$\Gamma_{\text{Cluster}} = A_1 \oplus A_2 \oplus 2E \tag{20}$$

of the Molecular Symmetry Group $C_{3v}(M)$ [4]. Those states of highest and lowest energy in each cluster span the $A_1 \oplus A_2$ representation; for even values of J the highest energy has A_1 symmetry and the lowest energy has A_2 symmetry, with the reverse true for odd J. The middle two states are represented by the doubly-degenerate E-type representation, giving a total of 6 ro-vibrational states for each energy cluster, resulting from (clockwise or anti-clockwise) rotation about three symmetrically equivalent axes, which become more pronounced as $J \to \infty$. Figure 7 only shows those states with the highest energies in each J manifold for clarity.

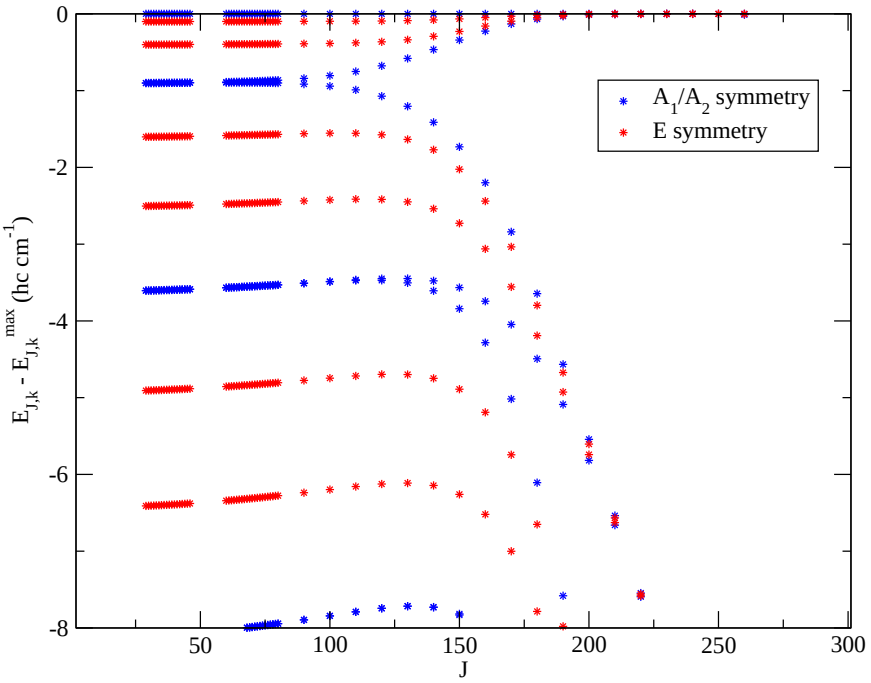

Figure 7. Rotational term value spacing, $\tilde{E}_{J,K} - \tilde{E}^{\max}_{J,K}$, as a function of J for the highest rotational energies in the ground vibrational state of PF_3. Blue stars represent states of A_1 or A_2 symmetries with red representing those of degenerate E symmetry, all part of the $C_{3v}(M)$ molecular symmetry group.

Clear evidence of rotational clustering can be seen in Figure 7; this occurs at a relatively high value of the rotational quantum number, around J=200. Table 2 gives a comparison with other XY_3 molecules.

Table 2. Values of rotational angular momentum J at which rotational energy clusters begin to form, for various XY_3 molecules. α_e gives the equilibrium bond angles between each Y atom.

Molecule	Cluster formation	Type	α_e	Reference
BiH_3	J=20	Pyramidal	91.6°	[47]
SbH_3	J=30	Pyramidal	91.5°	[47]
PH_3	J=50	Pyramidal	93.4°	[45]
PF_3	J=200	Pyramidal	98°	This work
SO_3	J=240	Planar	120°	[46]

The characteristics determining the energy, at which level clustering is expected to occur, are thought to be related to local-mode behaviour (see e.g. [97, 98]), with local-mode molecules exhibiting clustering behaviour more readily, at a lower rotational excitation. Local-mode behaviour is attributed specifically to XH_N molecules ($N = 2, 3, 4 \ldots$), with previously studied XH_3 molecules (in the context of rotational energy clustering), BiH_3 and SbH_3 [47], displaying strong local-mode behaviour. As shown in Table 2 these molecules consequently form rotational energy clusters at much lower rotational excitation than PF_3 and SO_3 [46]. PH_3 [45] has a less pronounced local-mode behaviour than BiH_3 or SbH_3, so exhibits cluster formation at a slightly higher rotational energy, but nevertheless much lower than for PF_3 and SO_3. BiH_3 is a typical local-mode molecule, with an equilibrium bond angle of 91.6° [99], a large mass ratio of M(Bi)/M(H), and small intermode coupling [97]. These almost orthonormal bonds make it ideally oriented for stable rotations. Although SbH_3 has similar local-mode properties to BiH_3, it has a less pronounced spherical top character, therefore forming rotational cluster states at a slightly higher rotational excitation.

5. Semi-Classical Analysis: Rotational Energy Surfaces

The first classical interpretation of these quasi-degenerate energy levels in spherical tops was formulated by Dorney and Watson in 1972 [100], inspiring many subsequent works [39, 52, 53, 101–113]. These investigations mostly revolve around the concept of a "localisation" axis for high rotational excitations and are characterised by a rotational energy surface (RES) [114]. The RES describes the classical (or semi-classical) rotational energy of a molecule as a function of the direction of the classical angular momentum vector in the molecule-fixed coordinate system, Euler angles θ and ϕ ($\theta \in [0°, 180°]$ and $\phi \in [0°, 360°]$), with a "quantum mechanical" length of $|\mathbf{J}| = \sqrt{J(J+1)}\hbar$ [47]; see Figure 8. A rotational energy surface is computed for different excitation levels of the rotational angular momenta, with corresponding stationary points coinciding with the formation of rotational energy clusters. As long as the molecule has structural symmetry, consisting of identical smaller atoms around a larger central atom, which are arranged symmetrically at equilibrium, then the localisation axes on the RES will also be symmetrical (the three symmetrically equivalent localisation axes are labelled as A on Figure 8, with clockwise and anticlockwise motion also equivalent for each). The phenomena is an interesting example of a quantum system tending towards becoming classical at a high energy. In this work we have employed an approach for the semi-classical analysis whereby the classical limit is applied to the ro-vibrational Hamiltonian and the classical energy subsequently minimised at each molecular orientation of the rotation, as was proposed by Harter [108]; details can be found elsewhere [41, 45, 46, 112].

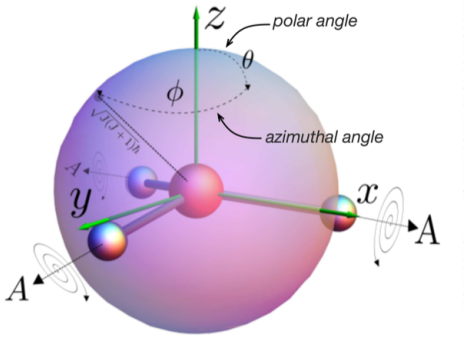

Figure 8. Illustration of the angles ($\theta \in [0°, 360°]$ and $\phi \in [0°, 180°]$) and classical angular momentum vector ($|\mathbf{J}| = \sqrt{J(J+1)}\hbar$) which constitute a rotational energy surface (RES) for PF_3 at a given value of J.

Figure 9 gives the progression of the 2D projection of the rotational energy surface of PF_3 with increasing values of J, as a function of θ and ϕ. The position of the largest (classical) energy value, in units of cm^{-1}, (in red, in the centre of the rotational energy plots) can be associated with a semi-classical limit of the quantum number k as $k = \sqrt{J(J+1)}\cos\theta$. For a given J, the classical energy varies with the angle θ in the same way as the quantum energy $\tilde{E}_{J,K}$ varies with the rotational quantum number K. The topology of the RES with six maxima, which form at $\theta = 90°$, $\phi = 30°, 90°, 150°, 210°, 270°$ and $330°$, is different from that found for XH_3 pyramidal molecules [45, 47, 112]. Namely the maxima at high J do not tend to roughly coincide with molecular bonds and are characterized by less pronounced barriers. This is however similar to the RES topology of SO_3 [46]. The clustering structure of Figure 7 is very similar in nature to both the XY_3-type and SO_3 molecules.

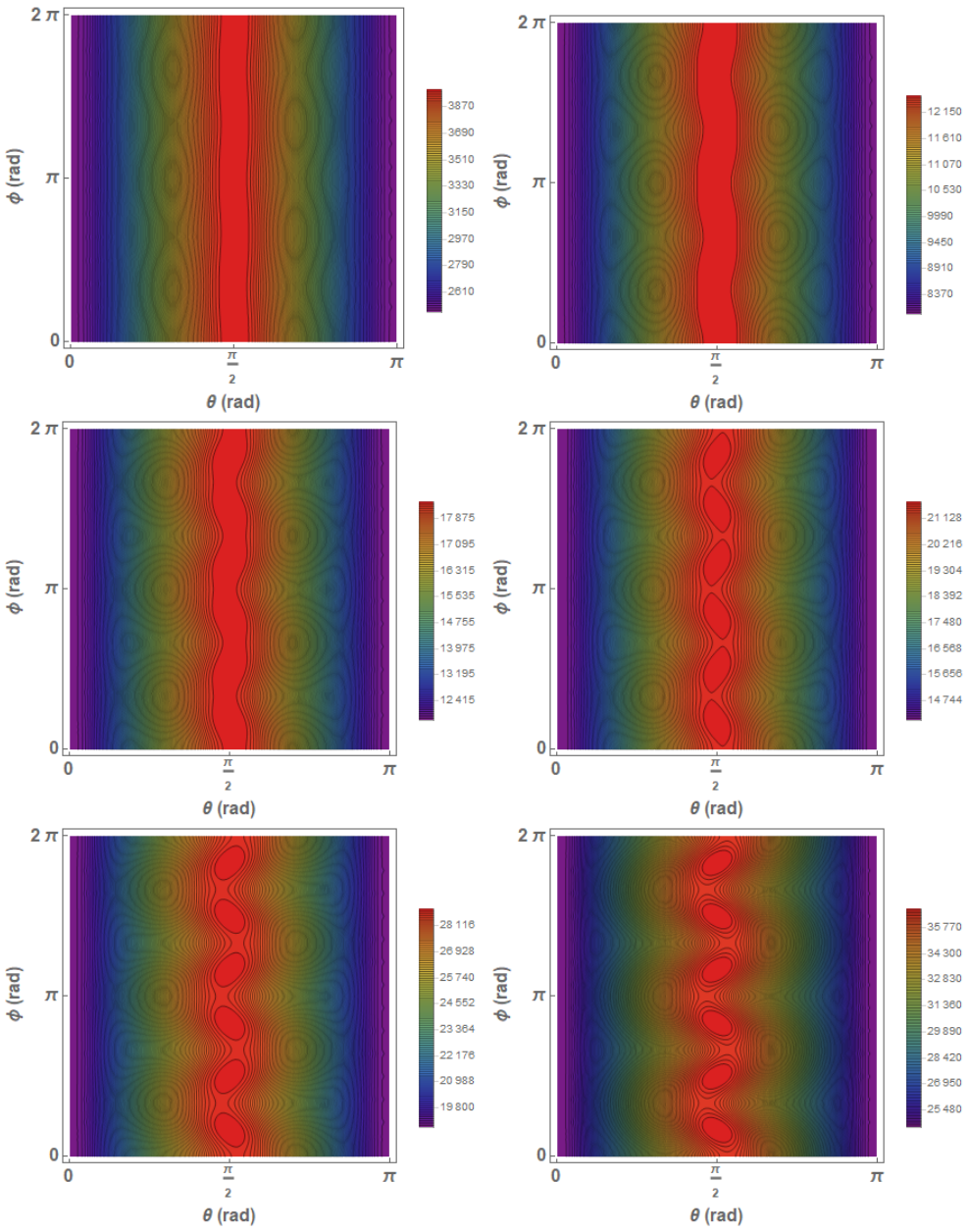

Figure 9. 2D projections of rotational energy surfaces $\tilde{E}_J(\theta, \phi)$ for PF_3 at increasing values of J (J=125, 225 (top row), 275, 300 (middle row), 350 and 400 (bottom row)).

6. Conclusions

We have computed new *ab initio* PES and DMS for the PF_3 molecule which were used to carry out variational nuclear motion calculations, simulate the infrared spectrum, and to perform an analysis of the rotational states at high rotational excitations. A clustering phenomena was found to occur which has been analysed using semi-classical methods and comparisons made with previous investigations into pyramidal spherical top molecules. It would be of interest to make further comparisons with even more

pyramidal molecules, NF_3 or AsH_3 [115] for example, in order to investigate the effects of molecular properties (such as mass, equilibrium bond angle, rotational constant, how rigid the molecule is) on the formation of rotational clustering states. An ideal molecule to study experimentally would be accessible at room-temperature. This would have clustering effects which begin to form at low rotational excitations, but should also have a low rotational constant, so that states of higher rotational excitation will be occupied for a particular temperature.

For PF_3, the rotational clustering occurs at around $J = 200$ (within 0.0x cm^{-1}), which corresponds to an energy of about $hc \times XXX.XX$ cm^{-1}. This is comparable to the clustering energy found in, for example PH3 (6300 cm^{-1}) [45]. Even though the rotational excitation is quite high, it does not have enough centrifugal energy to overcome the stiffness of the potential energy and form a stable rotation around one of the molecular bonds. Our search for the ideal clustering system will continue.

The *ab initio* calculated vibrational energies up to 3100 cm^{-1} are in reasonable agreement with experimental values. Rotational levels up to $J = 100$ were calculated and are in good agreement with the experimental values available.

Transition intensity calculations for up to $J = 100$ were carried out in order to simulate the room temperature spectrum. The calculations here could be readily extended to produce a hot PF_3 line list for the Exomol database, applicable for astronomical applications, if required. This would require states with much larger values of J (well over $J = 100$) to be included but techniques developed for SO_3 could be employed [46]. The room temperature PF_3 line list is available from the CDS (http://cdsarc.u-strasbg.fr) and ExoMol (www.exomol.com) data bases.

7. Disclosure statement

No potential conflict of interest was reported by the authors

Acknowledgements

This work was supported by the UK Science and Technology Research Council (STFC) No. ST/M001334/1, ST/R000476/1 and ST/J002925 and the COST action MOLIM No. CM1405. This work made extensive use of UCL's Legion and DARWIN and COSMOS high performance computing facilities provided by DiRAC for particle physics, astrophysics and cosmology and supported by STFC and BIS. A.Y. acknowledges support from DESY (HGF IVF) and from the excellence cluster "The Hamburg Center for Ultrafast Imaging—Structure, Dynamics and Control of Matter at the Atomic Scale" of the Deutsche Forschungsgemeinschaft (CUI, DFGEXC1074)

References

[1] R.J. Clark, H. Belefant and S.M. Williamson, Inorganic Syntheses **26**, 12–17 (1989).
[2] P. Bassett, D. Lloyd, I. Hillier and V. Saunders, Chemical Physics Letters **6**, 253 – 254 (1970).
[3] N.N. Greenwood and A. Earnshaw, *Chemistry of the Elements*, 2nd ed. (Butterworth-Heinemann, Oxford, 1997).
[4] P.R. Bunker and P. Jensen, *Fundamentals of Molecular Symmetry* (IOP Publishing, Bristol, 2004).

[5] T. Furtenbacher, P.A. Coles, J. Tennyson and A.G. Császár, J. Quant. Spectrosc. Radiat. Transf. (2017), To be submitted.
[6] S.N. Yurchenko, R.J. Barber, J. Tennyson, W. Thiel and P. Jensen, J. Mol. Spectrosc. **268**, 123–129 (2011).
[7] C. Sousa-Silva, A.F. Al-Refaie, J. Tennyson and S.N. Yurchenko, Mon. Not. R. Astron. Soc. **446**, 2337–2347 (2015).
[8] D.S. Marynick, J. Chem. Phys. **73** (8), 3939–3943 (1980).
[9] J.E. Boggs and D. Seida, J. Chem. Phys. **75** (7), 3645–3645 (1981).
[10] G.L. Gutsev **98**, 444 (1993).
[11] D.A. Dixon, A.J. Arduengo and T. Fukunaga, J. Am. Chem. Soc. **108**, 2461–2462 (1986).
[12] A. Owens, E.J. Zak, K.L. Chubb, S.N. Yurchenko, J. Tennyson and A. Yachmenev, Sci. Rep. **45068**, 7 (2017).
[13] C. Sousa-Silva, S.N. Yurchenko and J. Tennyson, J. Chem. Phys. **145**, 091102 (2016).
[14] M.K. Wilson and S.R. Polo, J. Chem. Phys. **20**, 1716–1719 (1952).
[15] A.M. Mirri, F. Scappini and P.G. Favero, Spectrochimica Acta **21**, 965–971 (1965).
[16] Y. Marino, K. Kuchitsu and T. Moritani, Inorg. Chem. **8** (4), 867–871 (1969).
[17] E. Hirota and Y. Morino, J. Mol. Spectrosc. **33**, 460–473 (1970).
[18] E. Hirota, J. Mol. Spectrosc. **37**, 20–32 (1971).
[19] E. Hirota, J. Mol. Spectrosc. **38**, 195–196 (1971).
[20] C.E. Small and J.G. Smith, J. Mol. Spectrosc. **73**, 215–233 (1978).
[21] H. Msahal, H. Najib and S. Hmimou, J. Mol. Spectrosc. **264**, 37–42 (2010).
[22] H. Najib and H. Msahal, Mol. Phys. **109** (15), 1953–1956 (2011).
[23] H. Najib, J. Mol. Spectrosc. **289**, 61–64 (2013).
[24] H. Najib, J. Mater. Environ. Sci. **4**, 721–725 (2013).
[25] H. Najib, J. Mol. Spectrosc. **305**, 17–21 (2014).
[26] A. Ceausu-Velcescu, P. Pracna, J. Breidung, W. Thiel and M. Badaoui, J. Mol. Spectrosc. **316**, 11 – 21 (2015).
[27] H. Najib, N. Ben Sari-Zizi, H. Būrger, A. Rahner and L. Halonen, J. Mol. Spectrosc. **159**, 249–258 (1993).
[28] N. Ben Sari-Zizi, H. Būrger, M. Litz, H. Najib and J. Radtke, J. Mol. Spectrosc. **177**, 46–57 (1996).
[29] E. Thiessen, J. Cosléou, P. Dréan, H. Harder, H. Mäder, L. Margulés, K. Sarka and U. Wötzel, J. Mol. Spectrosc. **517**, 91–103 (2000).
[30] M. Badaoui, N. Ben Sari-Zizi, H. Najib and G. Graner, J. Mol. Spectrosc. **184**, 318–329 (1997).
[31] N. Ben Sari-Zizi, H. Najib, R. Sebihi and P. Pracna, J. Mol. Spectrosc. **190**, 15–27 (1998).
[32] N. Ben Sari-Zizi, H. Najib, R. Sebihi and M. Badaoui, J. Mol. Spectrosc. **517**, 79–89 (2000).
[33] O.R. Gilliam, H.D. Edwards and W. Gordy, Phys. Rev. **75** (7), 1014 (1949).
[34] Y. Kawashima and A.P. Cox, J. Mol. Spectrosc. **65**, 319–329 (1977).
[35] G. Cotti, L. Cludi, L. Dore, G. Cazzoli and P. Dréan, J. Mol. Spectrosc. **174**, 78–84 (1995).
[36] M. Motamedi and T. Zohrevand, E-Journal of Chemistry **6** (3), 849–865 (2009).
[37] N. Hishiyama, M. Hoshino, F. Blanco, G. Garca and H. Tanaka, J. Chem. Phys. **148**, 084313 (2018).
[38] J. Breidung, W. Schneider, W. Thiel and H. Schafer, J. Mol. Spectrosc. **140**, 226–236 (1990).
[39] I.N. Kozin and I.M. Pavlichenkov, J. Chem. Phys. **104**, 4105–4113 (1996).
[40] I.N. Kozin and P. Jensen, J. Mol. Spectrosc. **163**, 483–509 (1994).
[41] I.N. Kozin and P. Jensen, J. Mol. Spectrosc. **161**, 186–207 (1993).
[42] J.M. Flaud, C. Camypeyret, H. Burger, P. Jensen and I.N. Kozin, J. Mol. Spectrosc. **172**, 126–134 (1995).
[43] P. Jensen, Y. Li, G. Hirsch, R.J. Buenker, T.J. Lee and I.N. Kozin, Chem. Phys. **190**,

179–189 (1995).
[44] P. Jensen, G. Osmann and I.N. Kozin, in *Advanced Series in Physical Chemistry: Vibration-Rotational Spectroscopy and Molecular Dynamics*, edited by D. Papousek, Vol. 9 (, , 1997), pp. 298–351.
[45] S.N. Yurchenko, W. Thiel, S. Patchkovskii and P. Jensen, Phys. Chem. Chem. Phys. **7**, 573–582 (2005).
[46] D.S. Underwood, S.N. Yurchenko, J. Tennyson and P. Jensen, J. Chem. Phys. **140**, 244316 (2014).
[47] S.N. Yurchenko, W. Thiel and P. Jensen, J. Mol. Spectrosc. **240**, 174–187 (2006).
[48] I.N. Kozin, S.P. Belov, O.L. Polyansky and M.Y. Tretyakov, J. Mol. Spectrosc. **152**, 13–28 (1992).
[49] J.M. Flaud, C. Camy-Peyret, H. Burger, P. Jensen and I.N. Kozin, J. Mol. Spectrosc. **172** (1), 126–134 (1995).
[50] S. Brodersen and B.I. Zhilinskiĭ, J. Mol. Spectrosc. **172**, 303–318 (1995).
[51] S. Brodersen and B.I. Zhilinskiĭ, J. Mol. Spectrosc. **169**, 1–17 (1995).
[52] D.A. Sadovskiĭ, B.I. Zhilinskiĭ, J.P. Champion and G. Pierre, J. Chem. Phys. **92**, 1523–1537 (1990).
[53] D.A. Sadovskiĭ and B.I. Zhilinskiĭ, Mol. Phys. **65**, 109–128 (1988).
[54] J.P. Aldridge, H. Filip, H. Flicker, R.F. Holland, R.S. McDowell, N.G. Nereson and K. Fox, J. Mol. Spectrosc. **58** (1), 165–168 (1975).
[55] A. Owens, A. Yachmenev, S.N. Yurchenko and J. Küpper, Phys. Rev. Lett. **121**, 193201 (2018).
[56] T. Adler, G. Knizia and H.J. Werner, J. Chem. Phys. **127**, 221106 (2007).
[57] K.A. Peterson, T.B. Adler and H.J. Werner, J. Chem. Phys. **128** (8), 084102 (2008).
[58] J.G. Hill, K.A. Peterson, G. Knizia and H.J. Werner, J. Chem. Phys. **131**, 194105 (2009).
[59] K.E. Yousaf and K.A. Peterson, J. Chem. Phys. **129**, 184108 (2008).
[60] F. Weigend, Phys. Chem. Chem. Phys. **4**, 4285–4291 (2002).
[61] C. Hättig, Phys. Chem. Chem. Phys. **7**, 59–66 (2005).
[62] H.J. Werner, P.J. Knowles, G. Knizia, F.R. Manby and M. Schütz, WIREs Comput. Mol. Sci. **2**, 242–253 (2012).
[63] S.N. Yurchenko, M. Carvajal, P. Jensen, F. Herregodts and T.R. Huet, Contemp. Phys. **290**, 59–67 (2003).
[64] R.I. Ovsyannikov, W. Thiel, S.N. Yurchenko, M. Carvajal and P. Jensen, J. Chem. Phys. **129**, 044309 (2008).
[65] C. Sousa-Silva, S.N. Yurchenko and J. Tennyson, J. Mol. Spectrosc. **288**, 28–37 (2013).
[66] S.N. Yurchenko, J.G. Zheng, H. Lin, P. Jensen and W. Thiel, J. Chem. Phys. **123**, 134308 (2005).
[67] S.N. Yurchenko, P.R. Bunker and P. Jensen, J. Molec. Struct. (THEOCHEM) **742**, 43–48 (2005).
[68] A.Y. Adam, A. Yachmenev, S.N. Yurchenko and P. Jensen, J. Chem. Phys. **143**, 244306 (2015).
[69] D.S. Underwood, J. Tennyson and S.N. Yurchenko, Phys. Chem. Chem. Phys. **15**, 10118–10125 (2013).
[70] S.N. Yurchenko, M. Carvajal, W. Thiel and P. Jensen, J. Mol. Spectrosc. **239**, 71–87 (2006).
[71] A. Taleb-Bendiab, M. LaBarge, L. Lohr, R. Taylor, K.H. II, R. Kuczkowski and R. Bohn, J. Chem. Phys. **90**, 6949 (1989).
[72] S.N. Yurchenko, W. Thiel and P. Jensen, J. Mol. Spectrosc. **245**, 126–140 (2007).
[73] S.N. Yurchenko, R.J. Barber, A. Yachmenev, W. Thiel, P. Jensen and J. Tennyson, J. Phys. Chem. A **113**, 11845–11855 (2009).
[74] A. Yachmenev and S.N. Yurchenko, J. Chem. Phys. **143**, 014105 (2015).
[75] S.N. Yurchenko, A. Yachmenev and R.I. Ovsyannikov, J. Chem. Theory Comput. **13**, 4368–4381 (2017).
[76] J. Tennyson and S.N. Yurchenko, Intern. J. Quantum Chem. **117**, 92–103 (2017).

[77] S.N. Yurchenko, R.J. Barber and J. Tennyson, Mon. Not. R. Astron. Soc. **413**, 1828–1834 (2011).
[78] O.L. Polyansky, I.N. Kozin, P. Maĺyszek, J. Koput, J. Tennyson and S.N. Yurchenko, J. Phys. Chem. A **117**, 7367–7377 (2013).
[79] S.N. Yurchenko and J. Tennyson, Mon. Not. R. Astron. Soc. **440**, 1649–1661 (2014).
[80] A.F. Al-Refaie, S.N. Yurchenko, A. Yachmenev and J. Tennyson, Mon. Not. R. Astron. Soc. **448**, 1704–1714 (2015).
[81] A.F. Al-Refaie, R.I. Ovsyannikov, O.L. Polyansky, S.N. Yurchenko and J. Tennyson, J. Mol. Spectrosc. **318**, 84–90 (2015).
[82] A. Owens, S.N. Yurchenko, A. Yachmenev, J. Tennyson and W. Thiel, J. Chem. Phys. **142**, 244306 (2015).
[83] D.S. Underwood, J. Tennyson, S.N. Yurchenko, A. Al-Refaie, S. Clausen and A. Fateev, Mon. Not. R. Astron. Soc. **462**, 4300–4313 (2016).
[84] A. Owens, S.N. Yurchenko, A. Yachmenev, W. Thiel and J. Tennyson, Mon. Not. R. Astron. Soc. **471**, 5025–5032 (2017).
[85] B.P. Mant, A. Yachmenev, J. Tennyson and S.N. Yurchenko, Mon. Not. R. Astron. Soc. **478**, 3220 – 3232 (2018).
[86] B.V. Noumerov, Mon. Not. Roy. Astron. Soc. **84**, 592–602 (1924).
[87] J.W. Cooley, Math. Comp. **15**, 363–374 (1961).
[88] H. Najib, Mol. Phys. **106**, 1199–1204 (2008).
[89] P.R. Bunker and P. Jensen, *Molecular Symmetry and Spectroscopy*, 2nd ed. (NRC Research Press, Ottawa, 1998).
[90] S.N. Yurchenko, W. Thiel, M. Carvajal, H. Lin and P. Jensen, Adv. Quant. Chem. **48**, 209–238 (2005).
[91] R.R. Gamache, C. Roller, E. Lopes, I.E. Gordon, L.S. Rothman, O.L. Polyansky, N.F. Zobov, A.A. Kyuberis, J. Tennyson, S.N. Yurchenko, A.G. Császár, T. Furtenbacher, X. Huang, D.W. Schwenke, T.J. Lee, B.J. Drouin, S.A. Tashkun, V.I. Perevalov and R.V. Kochanov, J. Quant. Spectrosc. Radiat. Transf. **203**, 70–87 (2017).
[92] A.F. Al-Refaie, J. Tennyson and S.N. Yurchenko, Comput. Phys. Commun. **214**, 216–224 (2017).
[93] S.N. Yurchenko, A.F. Al-Refaie and J. Tennyson, Astron. Astrophys. **614**, A131 (2018).
[94] M. Rey, I.S. Chizhmakova, A.V. Nikitin and V.G. Tyuterev, Phys. Chem. Chem. Phys. **20**, 21008–21033 (2018).
[95] S. Reichman and J. Overend, Spectrochimica Acta **26**, 379 – 389 (1970).
[96] S.W. Sharpe, T.J. Johnson, R.L. Sams, P.M. Chu, G.C. Rhoderick and P.A. Johnson, Applied Spec. **58**, 1452–1461 (2004).
[97] P. Jensen, Mol. Phys. **98** (17), 1253–1285 (2000).
[98] K.K. Lehmann, J. Chem. Phys. **95** (4), 2361–2370 (1991).
[99] L. Halonen and A.G. Robiette, J. Chem. Phys. **84** (12), 6861–6871 (1986).
[100] A.J. Dorney and J.K.G. Watson, J. Mol. Spectrosc. **42**, 135–148 (1972).
[101] W.G. Harter and C.W. Patterson, Int. J. Quant. Chem. **12**, 479–492 (1977).
[102] W.G. Harter and C.W. Patterson, J. Chem. Phys. **66**, 4872–4885 (1977).
[103] W.G. Harter and C.W. Patterson, Phys. Rev. Lett. **38**, 224–227 (1977).
[104] C.W. Patterson and W.G. Harter, J. Chem. Phys. **66**, 4886–4892 (1977).
[105] W.G. Harter and C.W. Patterson, J. Chem. Phys. **80**, 4241–4261 (1984).
[106] B.I. Zhilinskiĭ and I.M. Pavlichenkov, Zhurnal Eksperimentalnoi Teor. Fiz. **92**, 387–403 (1987).
[107] B.I. Zhilinsky and I.M. Pavlichenkov, Opt. Spektrosk. **64**, 688–690 (1988).
[108] W.G. Harter, Comp. Phys. Rep. **8**, 319–394 (1988).
[109] I.N. Kozin, R.M. Roberts and J. Tennyson, J. Chem. Phys. **111**, 140–150 (1999).
[110] B.I. Zhilinskiĭ, Phys. Rep.-Rev. Sec. Phys. Lett. **341**, 85–171 (2001).
[111] C. van Hecke, D.A. Sadovskiĭ, B.I. Zhilinskiĭ and V. Boudon, Eur. Phys. J. D **17**, 13–35 (2001).
[112] S.V. Petrov and B.M. Kozlovskii, J. Mol. Spectrosc. **243**, 245–252 (2007).

[113] W.G. Harter and J.C. Mitchell, Int. J. Mol. Sci. **14**, 714–806 (2013).
[114] W.G. Harter, Phys. Rev. A **24**, 192–263 (1981).
[115] P.A. Coles, S.N. Yurchenko, R.P. Kovacich, J. Hobby and J. Tennyson, Phys. Chem. Chem. Phys. (????).